Ligands Slow Down Pure-Dephasing in Semiconductor Quantum Dots

Jin Liu,[†] Svetlana V. Kilina,[‡] Sergei Tretiak,[§] and Oleg V. Prezhdo*[,∥]

[†]Department of Chemical Engineering, University of Rochester, Rochester, New York 14627, United States, [‡]Department of Chemistry, North Dakota State University, Fargo, North Dakota 58108, United States, [§]Los Alamos National Laboratory, Los Alamos, New Mexico 87545, United States, and [∥]Department of Chemistry, University of Southern California, Los Angeles, California 90089, United States

ABSTRACT It is well-known experimentally and theoretically that surface ligands provide additional pathways for energy relaxation in colloidal semiconductor quantum dots (QDs). They increase the rate of inelastic charge-phonon scattering and provide trap sites for the charges. We show that, surprisingly, ligands have the opposite effect on elastic electron−phonon scattering. Our simulations demonstrate that elastic scattering slows down in CdSe QDs passivated with ligands compared to that in bare QDs. As a result, the pure-dephasing time is increased, and the homogeneous luminescence line width is decreased in the presence of ligands. The lifetime of quantum superpositions of single and multiple excitons increases as well, providing favorable conditions for multiple excitons generation (MEG). Ligands reduce the pure-dephasing rates by decreasing phonon-induced fluctuations of the electronic energy levels. Surface atoms are most mobile in QDs, and therefore, they contribute greatly to the electronic energy fluctuations. The mobility is reduced by interaction with ligands. A simple analytical model suggests that the differences between the bare and passivated QDs persist for up to 5 nm diameters. Both low-frequency acoustic and high-frequency optical phonons participate in the dephasing processes in bare QDs, while low-frequency acoustic modes dominate in passivated QDs. The theoretical predictions regarding the pure-dephasing time, luminescence line width, and MEG can be verified experimentally by studying QDs with different surface passivation.

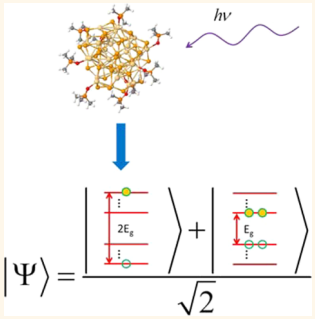

KEYWORDS: colloidal quantum dots · electron−phonon scattering · luminescence · multiple exciton generation · pure dephasing

Electron−phonon scattering plays key roles in the majority of processes taking place in semiconductor quantum dots (QDs), and other nanoscale and condensed phase materials. Most energy conversion processes (*e.g.*, light-to-electric) compete with energy losses to heat that occur *via* inelastic electron−phonon relaxation.[1−11] Elastic scattering leads to more subtle effects, which nevertheless play equally important roles. In particular, elastic electron−phonon scattering randomizes the phase of the electronic wave function, resulting in loss of quantum coherence.[12−15] Long-lived quantum coherences in biological and nanoscale systems are currently investigated for their role in light-harvesting function.[16,17] Even short-lived coherences are very important in quantum mechanics, because quantum transitions can occur only through a buildup of coherence. Rapid decoherence greatly slows down quantum dynamics, culminating in the quantum Zeno effect—complete termination of transitions in the limit of infinitely fast decoherence.[18] Loss of quantum coherence due to elastic electron−phonon scattering determines line widths of optical transitions, *via* the time-energy uncertainty relationship. In optics, decoherence phenomena are known as pure-dephasing.[19,20] Pure-dephasing rates determine the homogeneous contribution to the luminescence line width, which can be measured by a variety of spectroscopic probes.[21]

Both elastic and inelastic electron−phonon interactions are particularly important for solar energy harvesting. Here, achieving the highest photon-to-current conversion efficiency is paramount. However, the efficiency is limited by electron−phonon relaxation, resulting in the well-known Shockley-Queisser efficiency limit of 32%.[22] The remaining 68% of energy is either not absorbed or lost as heat. By slowing down electron-vibrational relaxation, one can attempt to extract hot excitons or charges[8,20,23,24] thus reducing energy losses. Even more intriguing is the possibility of using the excess energy to create

* Address correspondence to prezhdo@usc.edu.

Received for review May 29, 2015 and accepted August 18, 2015.

Published online August 18, 2015
10.1021/acsnano.5b03255

additional excitons *via* the process known as multiple exciton generation (MEG), observed in different types of QDs, including CdSe,[25] PbSe,[26,27] PbS,[28,29] Si,[30] InAs,[7] *etc*. Utilization of MEG raises the efficiency limit from 32% to 44%.[31]

A similar phenomenon, known as singlet fission (SF), transpires in molecular systems.[32−35] MEG occurs due to Coulomb coupling between singly and multiply excited states. The latter superpositions decohere (or dephase) due to elastic electron−phonon scattering. Thus, electron−phonon interactions influence MEG in a dual way. First, MEG competes with energy losses incurred as a result of inelastic electron−phonon scattering.[36] Second, the efficiency of MEG depends on the lifetime of coherent superpositions of single and multiple excitons, which is determined by elastic electron−phonon scattering.[13,37,38] As such, inelastic scattering lowers MEG efficiency due to rapid energy losses to heat, while strong elastic scattering decreases MEG efficiency by shortening lifetimes of coherent superpositions of single and multiple excitons, as exemplified by the quantum Zeno effect.[18]

The pioneering models describing the electronic wave function of the QD as a product of Bloch functions, capturing bulk properties, and an envelope function represent solution for an electron with an effective mass in a spherical well.[39−43] While simple EMA models are far from accurate and usually overemphasize the effects of quantum confinement by a large amount, EMA calculations do get better when multiple bands are included.[44] However, realistic samples of colloidal QDs are more complex and exhibit a variety of properties that can only be explained at the atomistic level of description. In particular, surface ligands have a strong influence on QD's photophysics. They prevent interdot interactions and reduce unsaturated valences on QD surfaces. Ligands also create trap states that can capture photoexcited electrons or holes, for instance, causing QDs to blink.[45,46] Since ligands are composed of lighter atoms, which have more conformational freedom, their vibrational modes are much faster and may strongly couple to the electronic degrees of freedom. Therefore, ligands can greatly accelerate electron−phonon relaxation and shorten lifetimes of electronic coherences.[2,47] Our previous study of electron−phonon relaxation in bare and passivated CdSe QDs showed that at excitation energies, 2.5 or more bandgaps (E_g), relevant for MEG, surface ligands accelerated the relaxation significantly.[24] At these energies, electronic states of ligands mix with QD states and effectively increase electron−phonon coupling. Analytic arguments demonstrate that the ligand effect persists even in QDs as large as 10 nm in diameter.

In this work we show, quite surprisingly, that QD ligands decrease the rate of elastic electron−phonon scattering, even though the inelastic scattering is accelerated in the same QDs. The difference arises for several reasons. *First*, electron−phonon relaxation at energies of $2.5E_g$ and above involves dense electronic states, which have significant ligand contributions. In contrast, the QD states forming quantum superposition that dephase due to elastic electron−phonon scattering have much less or no ligand contributions. In particular, optically allowed high energy singly excited states are mostly localized in the quantum dot core. Moreover, the multiply excited electronic states involved in MEG and composed by orbitals from the edges of the valence and conduction bands are also localized entirely inside QDs. Single excitons generated by light at high energies are localized inside QD cores due to optical selection rules.[24] In contrast, electron−phonon coupling obeys different selection rules, and high energy orbitals involved in nonradiative relaxation have significant ligand contributions.[24] *Second*, even though ligands provide a small contribution to the electronic density of the states near the bandgap, they strongly influence the energy fluctuation of such states. Specifically, ligands reduce mobility of QD surface atoms, which become stiffer with extra bonding and effectively heavier with attached ligands. *Third*, the electron−phonon couplings involved in inelastic and elastic scattering are not the same. The populations of electronic states are preserved during elastic scattering, and the electron−phonon coupling is adiabatic. In contrast, relaxation (or internal conversion) involves nonadiabatic coupling. Our simulations show that both low-frequency acoustic and high-frequency optical phonons facilitate pure-dephasing in bare QDs, while mostly low-frequency acoustic modes dominate in passivated QDs. An analytical model allows us to extrapolate the atomistic simulation results to larger QDs. It shows that the differences in the elastic electron−phonon scattering persist between bare and passivated QDs up to 5 nm in diameter. Notably, the differences in the inelastic scattering were significant in QDs with diameters up to 10 nm as shown in earlier work.[24] The ligand effect is more persistent with inelastic scattering due to direct involvement of ligands *via* electronic state delocalization. Our predicted differences in the pure-dephasing rates for bare and passivated QDs can be verified with photon−echo, luminescence line width, MEG yield, and related experiments on QDs with different surface passivation, involving bare QDs, various organic and inorganic ionic ligands, and core/shell structures.

RESULTS AND DISCUSSION

Geometric Structure. The study focuses on the bare and passivated $Cd_{33}Se_{33}$ QD of 1.3 nm in the diameter. Previously, QDs of this size range were not readily available for experiments due to challenging synthetic approaches. However, this situation is changing rapidly with the recent advances in the stable synthetic routes

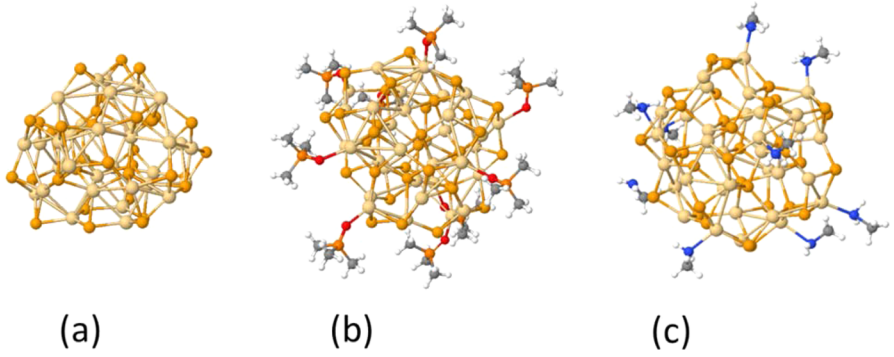

Figure 1. Structural snapshots of the bare and passivated QDs taken from the molecular dynamics trajectories at 300 K. (a) $Cd_{33}Se_{33}$; (b) $Cd_{33}Se_{33}$ + $9OPMe_3$; (c) $Cd_{33}Se_{33}$ + $9NH_2Me$.

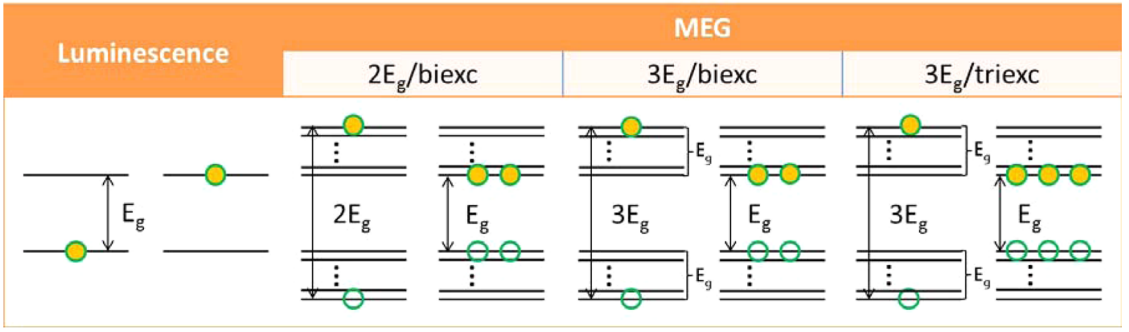

Figure 2. Illustration of the pure-dephasing processes considered here. Luminescence involves dephasing of the superposition between the first excited state and the ground state. MEG involves dephasing between single and multiple excitons, such as a double bandgap exciton and a biexciton ($2E_g$/biexc), a triple bandgap exciton and triexciton ($3E_g$/triexc), or a triple bandgap exciton and biexciton ($3E_g$/biexc). Various types of orbital excitations at a given energy (2, 2.5, and $3E_g$), both symmetric and asymmetric, are considered here. We computed the oscillator strength for each excitation and selected pairs of orbitals with the strongest oscillator strength. Symmetric excitation is typical of Pb salts, while it is asymmetric in CdSe.

for such nanoclusters.[48,49] The $Cd_{33}Se_{33}$ and Cd_{34} Se_{34} clusters have been observed is mass spectroscopy experiments showing to be extremely stable,[50] while also exhibiting remarkable optical properties.[48] $Cd_{33}Se_{33}$ is the smallest cluster that preserves crystalline structure of the bulk.[51,52] Clusters of this size are regularly obtained in colloidal solutions. These findings make $Cd_{33}Se_{33}$ an ideal candidate for modeling electronic and vibrational properties.

Mimicking most common QD passivations, we distributed evenly either nine phosphine oxides ($-OPMe_3$) or nine primary amines ($-NH_2Me_3$) on the $Cd_{33}Se_{33}$ surface. The structures of the bare and two passivated systems were described in details in our previous work.[24,52,53] Both types of ligands were carefully bound to the unsaturated surface Cd atoms, in agreement with the XPS experiments.[54] The experiments have shown that ligands such as trioctylphosphine oxide, thiophenol, α-toluenethiol, and *p*-hydroxythiophophenol bind much more strongly to Cd atoms than to Se atoms. Nine surface ligands passivate all two-coordinated Cd atoms in the current system. One can also consider passivation of all two- and three-coordinated Cd atoms. This requires 21 ligands. Addition of ligands greatly increases the computational effort. In particular, conformational flexibility of ligands demands longer trajectories for proper statistical sampling. Our previous studies have shown that the ligand effect on the optical response is qualitatively similar for partial passivation of the most reactive sites Cd (2-coordinated Cd) and full surface passivation.[52] The effect observed with 9 ligands in the present work should only become stronger with 21 ligands, and therefore, the results obtained with nine ligands properly characterize the observed effect.

Snapshots of the three model nanoclusters thermalized at 300 K are shown in Figure 1. All systems undergo surface reconstruction. The bond distances in the nanocrystals are different from those in CdSe bulk; nevertheless, the bulk-like binding topology is preserved. This is typical for nanocrystals, in which high surface-to-volume ratio signifies the role of surface atoms. It should be emphasized that the ligands do not change the overall shape and Cd−Se bonding pattern of the QD. The structure of the bare $Cd_{33}Se_{33}$ cluster is similar to the structures of the passivated clusters, indicating that the differences in the elastic electron−phonon scattering reported below arise due to ligands rather than passivation induced structural reconstruction of the CdSe core.

Electronic Structure. Figure 2 describes the pure-dephasing processes studied in this work. It shows the electronic states involved in the coherent superpositions

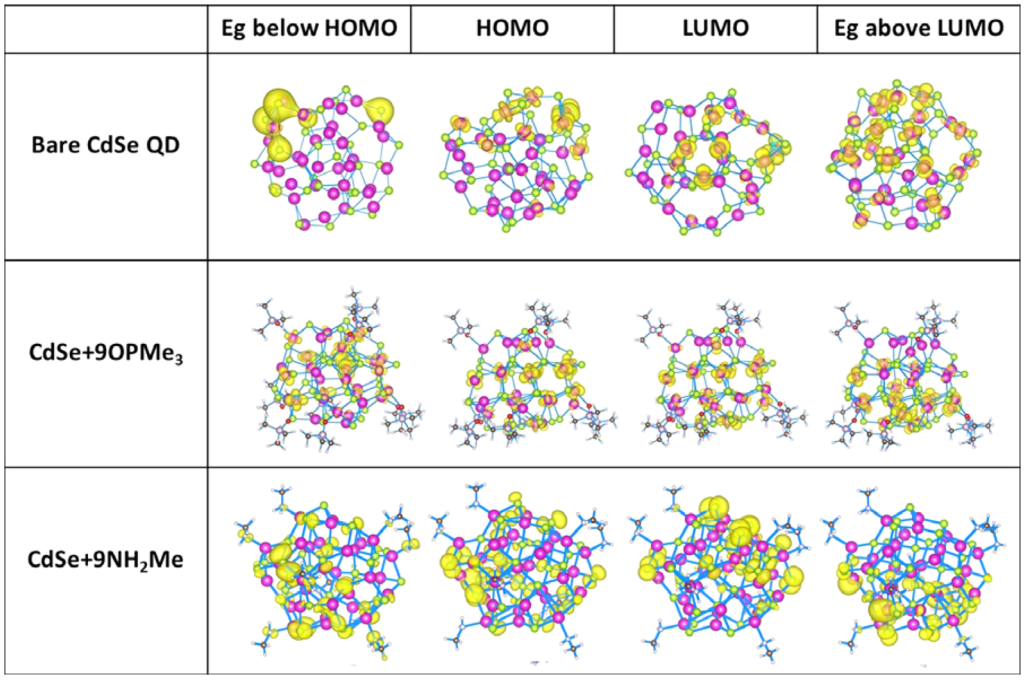

Figure 3. Charge densities of the four key electronic orbitals: orbital one-bandgap below HOMO, HOMO, LUMO and orbital one-bandgap above LUMO. Most orbitals are localized on the CdSe QD, indicating that the ligands are not directly involved in the electronic dynamics. All orbital density isosurfaces are set to the same value.

that are formed during luminescence and MEG, and that dephase by coupling to phonons. After dephasing, the two states become uncorrelated and evolve independently.[13,37,55] The leftmost panel depicts the ground and lowest excited states, which form a coherent superposition during luminescence. The pure-dephasing time for this pair determines the luminescence line width, $\Gamma \sim 1/T_2^*$, which can be probed by experiments. The other three plots in Figure 2 show various pairs of states that can form quantum superpositions during MEG. MEG can occur at different energies and can involve superpositions of both iso-energetic single and multiple excitons, and those having different energies. We selected the electronic orbitals forming coherent superpositions based on their optical activity.[24] Namely, we computed oscillator strengths of transitions between different pairs of orbitals at energies around 2, 2.5, and 3 times respective bandgaps, and selected the most optically active transitions. At the energy of $2E_g$, a bandgap biexciton can make a coherent mixture with a $2E_g$ single exciton. At $3E_g$, a bandgap triexciton can be in a superposition with a $3E_g$ single exciton. All these are iso-energetic superpositions. At the total energy of $2.5E_g$ and $3E_g$, single exciton can form coherence with a biexction formed by near bandgap states.

Figure 3 presents the spatial densities of the key electronic orbitals involved in the pure-dephasing processes considered here. Fluctuations of the energies of these orbitals during photodynamics determine the dephasing rates. Shown are the HOMO, LUMO, and typical orbitals forming optically active transitions localized away E_g from the band gap. The last ones form $3E_g$ single excitons. All orbitals are localized on CdSe in both bare and passivated QDs. This applies even to the high energy electron and hole orbitals that are one bandgap away from the HOMO and LUMO. According to ref 24, QD's core orbitals are most optically active for these nanostructures. The fact that both $OPMe_3$ and NH_2Me_3 ligands do not contribute substantially to the electronic density of the orbitals suggests that they should have a limited influence on the pure-dephasing processes. Surprisingly, this is not the case, as we show below.

Autocorrelation and Dephasing Functions. The pure-dephasing functions characterizing the luminescence and MEG processes are computed using the optical response formalism, as described in the Computational Methodology section. The dephasing times can be obtained by the second-order cumulant approximation or the direct method.[56] Both methods show similar results, while the second-order cumulant approximation offers more rapid convergence. The pure-dephasing times obtained using the cumulant approximation are reported in Figure 6.

The bare CdSe QD shows 3.7 fs homogeneous dephasing time for luminescence, corresponding to the 178 meV luminescence line width. The dephasing times for the passivated QDs increase to 6.7 fs, corresponding to the 99 meV line width. Quite unexpectedly, ligands slow down elastic electron−phonon scattering. Similarly, the pure-dephasing process destroying the superpositions of single and multiple excitons slows down in the presence of ligands.

Several groups reported luminescence data, focusing on the effect of QD size, temperature, and ligands. Extremely narrow line widths (5−8 meV) were discovered by fluorescence line narrowing experiments in homogeneous CdSe QDs at low temperature (10−15 K).[57−59] This narrow emission was attributed to frozen phonon modes at low temperature and homogeneous species. CdSe QD samples with a broader distribution of sizes and excitation energies produced luminescence with an ~65 meV full width at half-maximum.[44,58] At room temperature, corresponding to the temperature in our simulation, S. K. Buratto[60] observed 150 meV line width in 4.1 nm hexadecylamine-capped CdSe QD. Later, M. R. Salvador *et al.*[61] used the three-pulse echo peak shift method to quantify both homogeneous broadening caused by electron−phonon coupling, and inhomogeneous broadening arising from size distribution. The homogeneous line width was identified as 100 meV, compared to the 80 meV inhomogeneous line width. The most direct comparison between our calculation and experiment comes from the optical absorption measurements performed on CdSe clusters of the same size as in our calculation,[50] showing the line width of 147 meV. Our results on the bare (178 meV) and passivated (99 meV) CdSe QDs agree quite well with this experimental homogeneous broadening. Other three-pulse echo experiments[62] have indicated no significant difference in the line width data between phosphine oxide and amine capping ligands, agreeing with our calculations that show insignificant dependence of pure dephasing times on the ligand type.

The dephasing times (see Figure 6) defining the luminescence line width are substantially longer than those for MEGs. Similar theoretical predictions have been made for other types of QDs, such as PbSe[38] and Si.[13,55] This variance is attributed to significant differences in the electronic density distributions of the "hot" orbitals taking part in the MEG process, compared to those of the HOMO and LUMO involved in luminescence. For instance, LUMO has only one extra node than HOMO, while the orbitals composing high energy excitons involved in MEG and residing many orbitals away from the HOMO and LUMO have significantly different numbers of nodes. Generally, biexcitons create more perturbation toward the vibrational lattice and, therefore, couple to phonons more strongly than single excitons.[63]

Ligands and surface defects greatly influence dephasing processes in many materials. Here, ligands reduce the pure-dephasing rate. Our simulations of carbon nanotubes (CNT)[37] and graphene nanoribbons[64] have shown different dependence of dephasing in the presence of structural defects. In particular, defects introduce stronger coupling to local modes and accelerate dephasing in CNTs. In contrast, they slow down pure-dephasing in graphene ribbons, because the

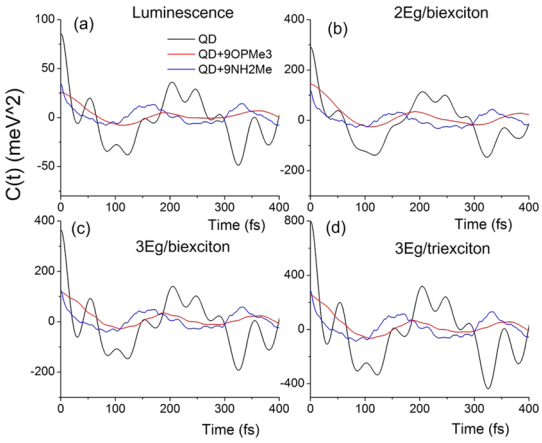

Figure 4. Un-normalized autocorrelation functions, $C_u(t)$ in eq 2, of the phonon-induced fluctuations of the gaps between the electronic energy levels involved in the luminescence and MEG processes of the bare CdSe QD (black line), $Cd_{33}Se_{33}$ (red line), and $Cd_{33}Se_{33} + 9NH_2Me$ (blue line). The initial values of the functions give the gap fluctuation squared. The gap fluctuations are notably larger for the bare QD than for the passivated QDs.

ribbons were able to relax the strain induced by the defect. QD ligands saturate surface dangling bonds, effectively removing defects and eliminating the strain in the QD structure, similarly to graphene nanoribbons.

To gain further insights into the origin of the pure-dephasing process in the bare and passivated QDs, we examine the unnormalized autocorrelation functions (ACFs) of the fluctuation in the electronic energy gaps. Unnormalized ACF is a convenient tool for analyzing time-domain repeating patterns in the signals. Under the cumulant approximation, the dephasing function is computed by integrating the unnormalized ACF, eq 5. A larger area under the ACF, achieved with a greater initial value and slower, smoother decay, favors faster dephasing. Figure 4 gives the unnormalized ACFs for all dephasing processes considered here. The *y*-axis scales are notably different in these plots. The scale is larger for MEG than that for luminescence. Also, the higher the energy of the states involved in MEG, the larger the scale (*e.g.*, contrast $2E_g$ *vs* $3E_g$, biexciton *vs* triexciton). Comparing bare and passivated QDs, we observe that the ACFs of the bare dots have larger initial values, while at the same time showing more oscillations between positive and negative regions. These two factors have opposite influence on the area under the ACF. Overall, the ACF amplitude is more important than its oscillation. As shown in Figure 3, ligands contribute little to the relevant molecular orbitals. The unnormalized AFCs shown in Figure 4 rationalize the ligand role. Ligands suppress fluctuations of the electronic energy levels by saturating surface dangling and increasing the effective mass of surface atoms.

The pure-dephasing functions obtained with the second-order cumulant expansion, eq 5, are plotted in

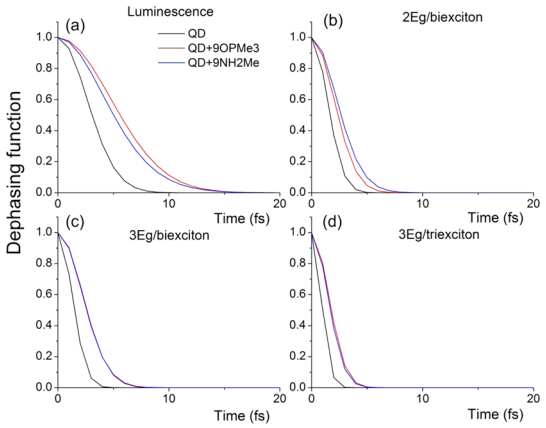

Figure 5. Pure-dephasing functions computed by the second-order cumulant expansion, eq 5, for the bare CdSe QD (black line), $Cd_{33}Se_{33}$ + 9OPMe$_3$ (red line), and $Cd_{33}Se_{33}$ + 9NH$_2$Me (blue line). The dephasing occurs faster in the bare QD.

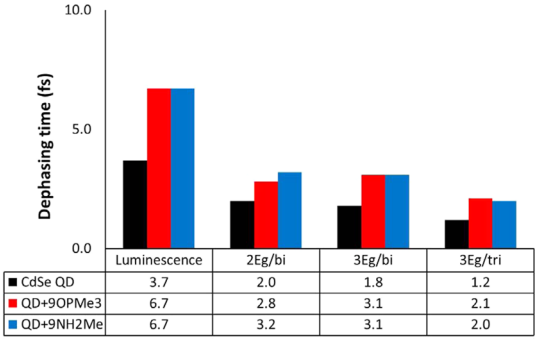

	Luminescence	2Eg/bi	3Eg/bi	3Eg/tri
CdSe QD	3.7	2.0	1.8	1.2
QD+9OPMe3	6.7	2.8	3.1	2.1
QD+9NH2Me	6.7	3.2	3.1	2.0

Figure 6. Pure-dephasing times for the luminescence and MEG processes in the bare and passivated CdSe QDs.

Figure 5. Each plot represents one type of dephasing process. The dephasing functions were fitted to Gaussians, $\exp(-t^2/2\tau^2)$, to obtain the dephasing times, τ, shown in Figure 6.

Phonon Modes. The phonon modes that contribute to the pure-dephasing processes are analyzed through Fourier transforms (FT) of the ACFs.[65−67] Shown in Figure 7, the FTs indicate that many more modes contribute to dephasing in bare $Cd_{33}Se_{33}$ compared to that in passivated $Cd_{33}Se_{33}$. Several different low frequency acoustic modes and high frequency optical modes are involved in the dephasing processes in bare $Cd_{33}Se_{33}$. In contrast, only one well-resolved peak at the frequency around 50 cm^{-1} associated with acoustic phonons and another large peak around 200 cm^{-1} corresponding to the longitudinal-optical (LO) phonon mode are responsible for dephasing in $Cd_{33}Se_{33}$ passivated with −OPMe$_3$ or −NH$_2$Me ligands. Note that changes in the size and capping groups have no effects on the LO frequency (207 cm^{-1}) in CdSe nanocrystals, as established experimentally.[62] This fact correlates well with our calculations. Participation of a much broader range of phonons rationalizes the rapid dephasing processes in the bare $Cd_{33}Se_{33}$ QD. The number

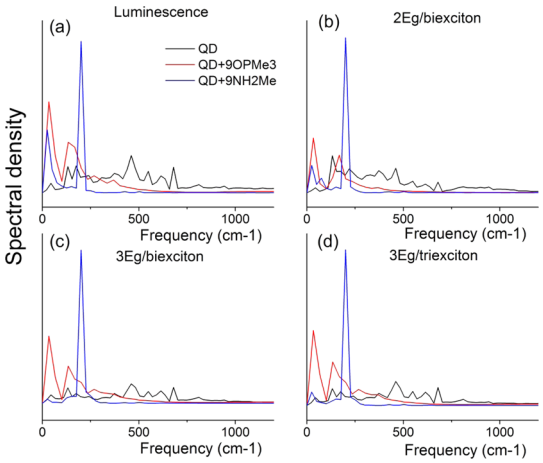

Figure 7. Spectral density calculated by Fourier transform, eq 3, of the autocorrelation functions for the bare CdSe QD (black line), $Cd_{33}Se_{33}$ + 9OPMe$_3$ (red line), and $Cd_{33}Se_{33}$ + 9NH$_2$Me (blue line). More phonon modes are involved in the dynamics of the bare CdSe.

TABLE 1. Standard Deviations in the Positions (Radii of Gyration) of Core and Surface Cd and Se Atoms in the Bare and Passivated QDs[a]

	all Cd	surface Cd	core Cd	all Se	surface Se	core Se
CdSe QD	0.56	0.57	0.51	0.51	0.52	0.40
CdSe + 9OPMe3	0.24	0.25	0.20	0.22	0.22	0.20
CdSe + 9NH2Me	0.19	0.19	0.15	0.17	0.18	0.13

[a] The data characterize spatial fluctuation of the atoms. Atoms in the passivated QDs move less than those in the bare CdSe, indicating that ligands help to stabilize the QD structure. Core atoms move less than surface atoms (unit: Å).

and positions of the peaks in the phonon influence spectra are almost the same for luminescence and MEG, indicating that the active phonon modes are the same in these different dephasing processes.

Additional information regarding the role of ligands in suppressing pure-dephasing is provided by the radii of gyration of the atoms, which characterize atom mobility. Specifically, we computed the standard deviation of the position of each atom i, $\sigma_i = [\langle(\vec{r}_{i,t} - \vec{r}_{i,\mathrm{mean}})^2\rangle_t]^{1/2}$. Here, $\vec{r}_{i,t}$ stands for the location of atom i at time t, and the angular bracket indicates ensemble averaging. A smaller standard deviation represents smaller fluctuation of that atom. We divided the Cd and Se atoms into core and surface subgroups based on the coordination number. Only 4-coordinated Cd and Se atoms are assigned to the core. Cd and Se atoms, which are 2- and 3-coordinated prior to ligand binding, are regarded as surface atoms. The standard deviations are listed in Table 1. The results indicate that the ligands significantly decrease the mobility of the atoms at room temperature: The standard deviations of both Cd and Se drop from over 0.5 Å in bare $Cd_{33}Se_{33}$ to about 0.2 Å in both passivated QDs. As expected, the core atoms move less than the surface atoms for all considered nanostructures. The decrease in atomic

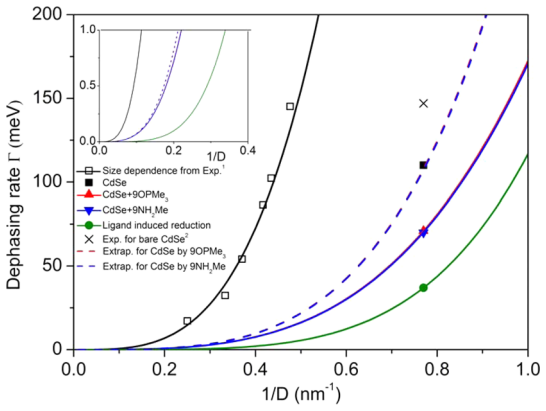

Figure 8. Analysis of the size-dependent ligand-induced reduction of the pure-dephasing rates for luminescence of CdSe QDs. The insert highlights the large diameter data. The black hollow squares are experimental data,[68] showing $1/D^{3.4}$ dependence of the pure-dephasing rate on QD diameter *D*. The rates are overestimated due to presence of defects. The cross shows the experimental[50] pure-dephasing rate for $Cd_{33}Se_{33}$ used in the current simulation. The filled square shows the pure-dephasing rate for bare $Cd_{33}Se_{33}$ calculated here, while the triangles show the calculated rates for passivated $Cd_{33}Se_{33}$. The circle represents the difference between the rates for the bare and passivated $Cd_{33}Se_{33}$, defining the ligand-induced reduction. The experimental[68] $1/D^{3.4}$ scaling obtained for passivated QDs is used to extrapolate the calculated data for the passivated $Cd_{33}Se_{33}$ to larger diameters. The ligand-induced reduction is scaled by both $1/D^{3.4}$ and the surface-to-volume ratio $1/D$. The extrapolation for the bare $Cd_{33}Se_{33}$ is obtained by combining the ligand-induced reduction with the passivated QD data. The analysis shows that ligands play an important role in QDs with diameters up to 5 nm.

fluctuations in capped QDs supports the fact that fewer phonon modes contribute to the dephasing processes in this case, Figure 7. As such, surface ligands stabilize QD structure and suppress vibrations.

Extrapolation to Larger Size. To estimate the importance of the pure-dephasing suppression induced by ligands to QDs of larger size, we build the following simple model, which is similar to our earlier consideration of the size-dependence of the relaxation process.[24] We separate the rate of the pure-dephasing process into contribution from the QD core and the ligands, $\Gamma = \Gamma_c + \Gamma_l$. Here, Γ is the inverse of the pure-dephasing time, and also has the meaning of the homogeneous luminescence line width. The pure-dephasing time of passivated CdSe QDs exhibits $1/D^{3.4}$ dependence on QD diameter *D*, according to the data of Figure 9 in ref 68. In addition, the ligand contribution to the rate should decrease according to the surface-to-volume ratio *S*/*V*, where $S \sim D^2$ and $V \sim D^3$. Thus, the scaling relationship for the ligand contribution can be written as $\Gamma_l = \Gamma_{l,0}(D/D_0)^{-4.4}$, where $\Gamma_{l,0}$ and D_0 are the ligand contribution to the dephasing rate and the QD diameter at a reference state.

Figure 8 shows the results of our scaling analysis. The experimental data[68] on the size dependence of the pure-dephasing rate in passivated CdSe QDs are shown by open squares. Here, the QD diameters are larger than those used in our simulation. The experimental rate is greater than the calculated values, due to contributions of solvent and defects, as discussed in the original publication.[68] The experimental data point (cross) reported in ref 50 for the QD of the same size as in our simulation is in good agreement with our data. The experimental rate is higher than the value calculated for the passivated QDs, likely due to solvent-induced pure-dephasing absent in the calculation, and possibly due to some sample inhomogeneity and defects present in experiment.

Overall, our simulations show that the ligands decrease the pure-dephasing rate. We scale the calculated pure-dephasing rate of the passivated QDs using the experimentally[68] determined law, $1/D^{3.4}$ (red and blue lines in Figure 8) and the ligand-induced decrease by the law, $1/D^{4.4}$, accounting for the surface-to-volume ratio (green line in Figure 8). Added together, these two curves produce the size-dependent dephasing rate for the bare QD (dashed lines in Figure 8). The plots show that ligands strongly affect the pure-dephasing rate in small QDs. The ligand contribution decreases gradually to reach about 10% in 5 nm QDs (see Figure 8, inset). Comparing the outcome of the above analysis of pure-dephasing with a similar analysis of the electron−phonon relaxation,[24] we conclude that overall, ligand contributions are significant even in relatively large QDs. At the same time, the influence of ligands on pure-dephasing is somewhat weaker and has the opposite effect than on nonradiative relaxation. The latter process occurs in a stepwise fashion including electronic states that are close in energy. Many of these states are hybridized between the QD and ligands. On the other hand, pure-dephasing involves pairs of high and low energy orbitals, which are mainly localized on the QD and have no ligand contribution. These "core" orbitals are involved in the pure-dephasing, because they give high oscillator strength for optical transitions. Additionally, the ligand effect on pure-dephasing is indirect, *via* modification of the spatial fluctuations of surface atoms.

CONCLUSIONS

In summary, this work examined computationally phonon-induced pure-dephasing processes in bare $Cd_{33}Se_{33}$ and $Cd_{33}Se_{33}$ capped with $-OPMe_3$ or $-NH_2Me$ ligands. The focus was on the elastic electron−phonon scattering that determines luminescence line widths and lifetimes of superpositions of single and multiple excitons formed during MEGs. Ligands slow down pure-dephasing rates, decreasing luminescence line widths and increasing the MEG superposition lifetimes. The result is somewhat unexpected, since the previous study of energy relaxation in the same QDs showed ligand-induced acceleration of inelastic

electron−phonon scattering. The difference is rationalized by the fact that ligands have no direct contributions to the electronic densities of the optically active states involved in the photogenerated singly and multiply excited state superpositions. Additionally, ligands indirectly reduce fluctuations of the QD atoms and, thus, increase coherence time. In contrast, the higher-energy electronic states involved in the relaxation are delocalized onto ligands, and therefore, the latter effectively increase the electron−phonon coupling in the case of inelastic processes.

Our calculations of the pure-dephasing times that determine luminescence line widths at 300 K give 4 fs for bare $Cd_{33}Se_{33}$ and 7 fs for the passivated QDs. These values agree well with the experimentally available line widths. The dephasing associated with MEG is faster, because MEG involves biexcitons, which create stronger electron−phonon coupling than excitons, and because the orbitals supporting superpositions of single and multiple excitons during MEG differ more significantly (*e.g.*, in the number of nodes) than the HOMO and LUMO involved in luminescence.

Phonon mode analysis indicates that a wide range of both low-frequency acoustic and high-frequency optical modes participate in the dephasing processes in bare $Cd_{33}Se_{33}$, while many fewer modes with the dominating contribution from low-frequency acoustic phonons are active in the ligand passivated $Cd_{33}Se_{33}$ QDs. The ligands stabilize the $Cd_{33}Se_{33}$ core, largely eliminating high-frequency vibrational motions. While surface ligands do not couple to the charge dynamics directly, they restrict motions of the QD atoms, thus making the dephasing processes longer. Analysis of displacements of the Cd and Se atoms located in different parts of the QDs supports this conclusion quantitatively. Ligands reduce the radii of gyration of Cd and Se atoms by more than a factor of 2, with surface atoms receiving a more significant reduction.

A simple analytic model of the size-dependence of the ligand contribution to the pure-dephasing processes shows that the ligand effect extends to QDs up to 5 nm in diameter, in which case ligands reduce the dephasing rate by 10%.

The predicted changes in the pure-dephasing times and luminescence line widths can be tested experimentally by investigation of QDs of different size and surface passivation, including organic and inorganic ligands, bare clusters, and core/shell structures.

COMPUTATIONAL METHODOLOGY

Optical Response, Pure-Dephasing Function. The phonon-induced pure-dephasing times associated with the luminescence and MEG processes are computed using the optical response function formalism.[56] If we exclude inhomogeneous broadening associated with a distribution of optically active species, the homogeneous line width Γ is inversely proportional to the dephasing time, T_2, which includes the excited state lifetime, T_1 and the pure-dephasing time, T_2^*.

$$\Gamma = \frac{1}{T_2} = \frac{1}{2T_1} = \frac{1}{T_2^*} \tag{1}$$

For a sufficiently long lifetime, T_1, which is common for near bandgap excitations, Γ is determined solely by T_2^*.[69]

Pure-dephasing is associated with fluctuations of electronic energy levels due to coupling to either phonons or environment. Since we do not consider any solvent around the QDs in the present study, the dephasing is only caused by phonons of the QDs and the ligands. The fluctuations are characterized by the energy gap autocorrelation function (ACF). The normalized ACF is defined as

$$C(t) = \frac{\langle \Delta E(t)\Delta E(0)\rangle}{\langle \Delta E^2(0)\rangle} = \frac{C_u(t)}{\langle \Delta E^2(0)\rangle} \tag{2}$$

where $C_u(t)$ is the unnormalized ACF. The initial value of the unnormalized ACF, $C_u(0)$, gives the energy gap fluctuation squared. The averaging is performed over the canonical ensemble. The ACFs characterize the memory of the energy gap fluctuation. A rapid decay of the ACFs implies fast pure-dephasing. A large gap fluctuation, characterized by $C_u(0)$, also leads to fast pure-dephasing.

Fourier transform of the ACF produces the spectral density,

$$I(\omega) = \left| \frac{1}{\sqrt{2\pi}} \int_{-\infty}^{\infty} dt e^{-iwt} C(t) \right|^2 \tag{3}$$

which identifies the phonon modes involved in the dephasing process. The peaks of the spectra indicate the strength of the electron−phonon coupling for the phonon modes of given frequencies. Multiple frequencies present in the spectral density usually lead to a rapid ACF decay.

The optical response function considered below characterizes the pure-dephasing process for a pair of states entangled in a coherent superposition. It can be obtained directly or *via* the second-order cumulant expansion.[56] The direct dephasing function is computed as,

$$D(t) = \exp(i\omega t)\left\langle \exp\left(-\frac{i}{\hbar}\int_0^t d\tau \Delta E(\tau)\right)\right\rangle \tag{4}$$

The second-order cumulant expansion of eq 4 leads to

$$D(t) = \exp(-g(t)), \quad g(t) = \frac{1}{\hbar^2}\int_0^t d\tau_1 \int_0^{\tau_1} d\tau_2 C_u(\tau_2) \tag{5}$$

The cumulant expression indicates that dephasing is rapid if the integrated $C_u(t)$ is large. This is achieved when $C_u(t)$ decays slowly and does not change sign, and when its initial value $C_u(0)$, corresponding to the standard deviation in the energy gap, is large. The cumulant function (eq 5) converges faster than the direct expression (eq 4), because the latter involves averaging of a complex-valued oscillatory function, whose real and imaginary parts change signs.

***Ab Initio* Molecular Dynamics.** The atomistic simulation reported here were performed in the framework of density functional theory implemented with the Vienna *Ab initio* Simulation Package (VASP).[70] The simulation protocol was the same as in our earlier study.[6,11,24,71] The generalized-gradient approximation (GGA) density functional of Perdew and Wang (PW91),[72,73] coupled with the Vanderbilt pseudopotential,[74] was employed. Periodic cubic cells with 9 Å of vacuum around the QDs, and converged plane wave basis set were used. After geometry optimization by the conjugate-gradient algorithm, the QD structures were heated to 300 K with repeated velocity rescaling. Microcanonical molecular dynamics (MD) trajectories of 1−1.5 ps duration were generated for each temperature and for each system, using the Verlet algorithm with the 1 fs time step relying on Hellman-Feynman forces. The optimization, heating

and microcanonical MD showed no major changes in the atomic and electronic structure, such as bond breaking or fragmentation. The dephasing times for the luminescence and MEG processes were computed based on the MD trajectories using eqs 4 and 5. It is assumed that electron-vibrational interaction depends weakly on explicit electron−hole Coulomb interactions. Note that electron correlations effects are included implicitly in the DFT functional. The influence of explicit electron−hole interaction on electron-vibrational coupling is a higher order effect and is weak. In particular, we carried out tests by comparing the results of Kohn−Sham and linear-response TDDFT calculations with semiconductor QDs and other systems using various DFT functional.[52,53,65,75] The calculations showed that the phonon-induced fluctuations in the electronic energy levels, which characterize the strength of the electron-vibrational coupling, are practically indistinguishable for the two methods, with and without explicit electron−hole correlation.

Conflict of Interest: The authors declare no competing financial interest.

Acknowledgment. J.L. and O.V.P. acknowledge financial support of the U.S. Department of Energy Grant No. DE-SC0014429. S.V.K. acknowledges financial support of the U.S. Department of Energy (DOE) Early Career Research Grant No. DE-SC008446. The authors are grateful for support from the user facility of the Center for Integrated Nanotechnologies (CINT) at Los Alamos National Laboratory.

REFERENCES AND NOTES

1. Geiregat, P.; Delerue, C.; Justo, Y.; Aerts, M.; Spoor, F.; Van Thourhout, D.; Siebbeles, L. D. A.; Allan, G.; Houtepen, A. J.; Hens, Z. A Phonon Scattering Bottleneck for Carrier Cooling in Lead Chalcogenide Nanocrystals. *ACS Nano* **2015**, *9*, 778–788.
2. Pandey, A.; Guyot-Sionnest, P. Slow Electron Cooling in Colloidal Quantum Dots. *Science* **2008**, *322*, 929–932.
3. Kilina, S. V.; Kilin, D. S.; Prezhdo, O. V. Breaking the Phonon Bottleneck in PbSe and CdSe Quantum Dots: Time-Domain Density Functional Theory of Charge Carrier Relaxation. *ACS Nano* **2009**, *3*, 93–99.
4. Gao, J. B.; Zhang, J. B.; van de Lagemaat, J.; Johnson, J. C.; Beard, M. C. Charge Generation in PbS Quantum Dot Solar Cells Characterized by Temperature-Dependent Steady-State Photoluminescence. *ACS Nano* **2014**, *8*, 12814–12825.
5. Lin, C.; Kelley, D. F.; Rico, M.; Kelley, A. M. The "Surface Optical" Phonon in CdSe Nanocrystals. *ACS Nano* **2014**, *8*, 3928–3938.
6. Neukirch, A. J.; Guo, Z. Y.; Prezhdo, O. V. Time-Domain *Ab initio* Study of Phonon-Induced Relaxation of Plasmon Excitations in a Silver Quantum Dot. *J. Phys. Chem. C* **2012**, *116*, 15034–15040.
7. Schaller, R. D.; Pietryga, J. M.; Klimov, V. I. Carrier Multiplication in InAs Nanocrystal Quantum Dots with an Onset Defined by the Energy Conservation Limit. *Nano Lett.* **2007**, *7*, 3469–3476.
8. Long, R.; Prezhdo, O. V. *Ab initio* Nonadiabatic Molecular Dynamics of the Ultrafast Electron Injection from a PbSe Quantum Dot into the TiO2 Surface. *J. Am. Chem. Soc.* **2011**, *133*, 19240–19249.
9. Yeltik, A.; Guzelturk, B.; Hernandez-Martinez, P. L.; Govorov, A. O.; Demir, H. V. Phonon-Assisted Exciton Transfer into Silicon Using Nanoemitters: The Role of Phonons and Temperature Effects in Forster Resonance Energy Transfer. *ACS Nano* **2013**, *7*, 10492–10501.
10. Hyeon-Deuk, K.; Prezhdo, O. V. Multiple Exciton Generation and Recombination Dynamics in Small Si and CdSe Quantum Dots: An *ab initio* Time-Domain Study. *ACS Nano* **2012**, *6*, 1239–1250.
11. Liu, J.; Neukirch, A. J.; Prezhdo, O. V. Non-Radiative Electron−Hole Recombination in Silicon Clusters: *Ab initio* Non-Adiabatic Molecular Dynamics. *J. Phys. Chem. C* **2014**, *118*, 20702–20709.
12. Neal, A. T.; Liu, H.; Gu, J. J.; Ye, P. D. D. Magneto-transport in MoS2: Phase Coherence, Spin-Orbit Scattering, and the Hall Factor. *ACS Nano* **2013**, *7*, 7077–7082.
13. Madrid, A. B.; Hyeon-Deuk, K.; Habenicht, B. F.; Prezhdo, O. V. Phonon-Induced Dephasing of Excitons in Semiconductor Quantum Dots: Multiple Exciton Generation, Fission, and Luminescence. *ACS Nano* **2009**, *3*, 2487–2494.
14. Yuen-Zhou, J.; Arias, D. H.; Eisele, D. M.; Steiner, C. P.; Krich, J. J.; Bawendi, M. G.; Nelson, K. A.; Aspuru-Guzik, A. Coherent Exciton Dynamics in Supramolecular Light-Harvesting Nanotubes Revealed by Ultrafast Quantum Process Tomography. *ACS Nano* **2014**, *8*, 5527–5534.
15. Jaeger, H. M.; Fischer, S.; Prezhdo, O. V. Decoherence-Induced Surface Hopping. *J. Chem. Phys.* **2012**, *137*, 22A545.
16. Herek, J. L.; Wohlleben, W.; Cogdell, R. J.; Zeidler, D.; Motzkus, M. Quantum Control of Energy Flow in Light Harvesting. *Nature* **2002**, *417*, 533–535.
17. Collini, E.; Wong, C. Y.; Wilk, K. E.; Curmi, P. M. G.; Brumer, P.; Scholes, G. D. Coherently Wired Light-Harvesting in Photosynthetic Marine Algae at Ambient Temperature. *Nature* **2010**, *463*, 644–647.
18. Kilina, S. V.; Neukirch, A. J.; Habenicht, B. F.; Kilin, D. S.; Prezhdo, O. V. Quantum Zeno Effect Rationalizes the Phonon Bottleneck in Semiconductor Quantum Dots. *Phys. Rev. Lett.* **2013**, *110*, 180404.
19. Abramavicius, D.; Palmieri, B.; Voronine, D. V.; Sanda, F.; Mukamel, S. Coherent Multidimensional Optical Spectroscopy of Excitons in Molecular Aggregates; Quasiparticle *versus* Supermolecule Perspectives. *Chem. Rev.* **2009**, *109*, 2350–2408.
20. Prezhdo, O. V. Photoinduced Dynamics in Semiconductor Quantum Dots: Insights from Time-Domain *ab initio* Studies. *Acc. Chem. Res.* **2009**, *42*, 2005–2016.
21. Liu, W.; Zhang, Y.; Zhai, W.; Wang, Y.; Zhang, T.; Gu, P.; Chu, H.; Zhang, H.; Cui, T.; Wang, Y.; et al. Temperature-Dependent Photoluminescence of ZnCuInS/ZnSe/ZnS Quantum Dots. *J. Phys. Chem. C* **2013**, *117*, 19288–19294.
22. Shockley, W.; Queisser, H. J. Detailed Balance Limit of Efficiency of P-N Junction Solar Cells. *J. Appl. Phys.* **1961**, *32*, 510–519.
23. Prezhdo, O. V.; Duncan, W. R.; Prezhdo, V. V. Photoinduced Electron Dynamics at the Chromophore-Semiconductor Interface: A Time-Domain *ab initio* Perspective. *Prog. Surf. Sci.* **2009**, *84*, 30–68.
24. Kilina, S.; Velizhanin, K. A.; Ivanov, S.; Prezhdo, O. V.; Tretiak, S. Surface Ligands Increase Photoexcitation Relaxation Rates in CdSe Quantum Dots. *ACS Nano* **2012**, *6*, 6515–6524.
25. Schaller, R. D.; Petruska, M. A.; Klimov, V. I. Effect of Electronic Structure on Carrier Multiplication Efficiency: Comparative Study of PbSe and CdSe Nanocrystals. *Appl. Phys. Lett.* **2005**, *87*, 253102–253104.
26. Tisdale, W. A.; Williams, K. J.; Timp, B. A.; Norris, D. J.; Aydil, E. S.; Zhu, X.-Y. Hot-Electron Transfer from Semiconductor Nanocrystals. *Science* **2010**, *328*, 1543–1547.
27. Semonin, O. E.; Luther, J. M.; Choi, S.; Chen, H.-Y.; Gao, J.; Nozik, A. J.; Beard, M. C. Peak External Photocurrent Quantum Efficiency Exceeding 100% *via* MEG in a Quantum Dot Solar Cell. *Science* **2011**, *334*, 1530–1533.
28. Sambur, J. B.; Novet, T.; Parkinson, B. A. Multiple Exciton Collection in a Sensitized Photovoltaic System. *Science* **2010**, *330*, 63–66.
29. Gdor, I.; Sachs, H.; Roitblat, A.; Strasfeld, D. B.; Bawendi, M. G.; Ruhman, S. Exploring Exciton Relaxation and Multiexciton Generation in PbSe Nanocrystals Using Hyperspectral Near-IR Probing. *ACS Nano* **2012**, *6*, 3269–3277.
30. Beard, M. C.; Knutsen, K. P.; Yu, P.; Luther, J. M.; Song, Q.; Metzger, W. K.; Ellingson, R. J.; Nozik, A. J. Multiple Exciton Generation in Colloidal Silicon Nanocrystals. *Nano Lett.* **2007**, *7*, 2506–2512.
31. Hanna, M. C.; Nozik, A. J. Solar Conversion Efficiency of Photovoltaic and Photoelectrolysis Cells with Carrier Multiplication Absorbers. *J. Appl. Phys.* **2006**, *100*, 074510.
32. Chan, W. L.; Ligges, M.; Jailaubekov, A.; Kaake, L.; Miaja-Avila, L.; Zhu, X.-Y. Observing the Multiexciton State in Singlet Fission and Ensuing Ultrafast Multielectron Transfer. *Science* **2011**, *334*, 1541–1545.
33. Bange, S.; Scherf, U.; Lupton, J. M. Absence of Singlet Fission and Carrier Multiplication in a Model Conjugated

Polymer: Tracking the Triplet Population through Phosphorescence. *J. Am. Chem. Soc.* **2012**, *134*, 1946–1949.
34. Wang, L.; Olivier, Y.; Prezhdo, O. V.; Beljonne, D. Maximizing Singlet Fission by Intermolecular Packing. *J. Phys. Chem. Lett.* **2014**, *5*, 3345–3353.
35. Akimov, A. V.; Prezhdo, O. V. Nonadiabatic Dynamics of Charge Transfer and Singlet Fission at the Pentacene/C60 Interface. *J. Am. Chem. Soc.* **2014**, *136*, 1599–1608.
36. Mangum, B. D.; Wang, F.; Dennis, A. M.; Gao, Y.; Ma, X.; Hollingsworth, J. A.; Htoon, H. Competition between Auger Recombination and Hot-Carrier Trapping in PL Intensity Fluctuations of Type II Nanocrystals. *Small* **2014**, *10*, 2892–2901.
37. Habenicht, B. F.; Kamisaka, H.; Yamashita, K.; Prezhdo, O. V. *Ab initio* Study of Vibrational Dephasing of Electronic Excitations in Semiconducting Carbon Nanotubes. *Nano Lett.* **2007**, *7*, 3260–3265.
38. Kamisaka, H.; Kilina, S. V.; Yamashita, K.; Prezhdo, O. V. Ultrafast Vibrationally-Induced Dephasing of Electronic Excitations in PbSe Quantum Dots. *Nano Lett.* **2006**, *6*, 2295–2300.
39. Brus, L. E. On the Development of Bulk Optical Properties in Small Semiconductor Crystallites. *J. Lumin.* **1984**, *31−32*, 381–384.
40. Brus, L. Electronic Wave Functions in Semiconductor Clusters: Experiment and Theory. *J. Phys. Chem.* **1986**, *90*, 2555–2560.
41. Bawendi, M. G.; Steigerwald, M. L.; Brus, L. E. The Quantum Mechanics of Larger Semiconductor Clusters (″ Quantum Dots″). *Annu. Rev. Phys. Chem.* **1990**, *41*, 477–496.
42. Ekimov, A. I.; Kudryavtsev, I. A.; Efros, A. L.; Yazeva, T. V.; Hache, F.; Schanne-Klein, M. C.; Rodina, A. V.; Ricard, D.; Flytzanis, C. Absorption and Intensity-Dependent Photoluminescence Measurements on CdSe Quantum Dots: Assignment of the First Electronic Transitions. *J. Opt. Soc. Am. B* **1993**, *10*, 100–107.
43. Efros, A. L.; Rosen, M.; Kuno, M.; Nirmal, M.; Norris, D. J.; Bawendi, M. Band-edge Exciton in Quantum Dots of Semiconductors with a Degenerate Valence Band: Dark and Bright Exciton States. *Phys. Rev. B: Condens. Matter Mater. Phys.* **1996**, *54*, 4843–4856.
44. Norris, D. J.; Bawendi, M. G. Measurement and Assignment of the Size-Dependent Optical Spectrum in CdSe Quantum Dots. *Phys. Rev. B: Condens. Matter Mater. Phys.* **1996**, *53*, 16338–16346.
45. Zhang, A.; Dong, C.; Liu, H.; Ren, J. Blinking Behavior of CdSe/CdS Quantum Dots Controlled by Alkylthiols as Surface Trap Modifiers. *J. Phys. Chem. C* **2013**, *117*, 24592–24600.
46. Schmidt, R.; Krasselt, C.; Göhler, C.; von Borczyskowski, C. The Fluorescence Intermittency for Quantum Dots Is Not Power-Law Distributed: A Luminescence Intensity Resolved Approach. *ACS Nano* **2014**, *8*, 3506–3521.
47. Guyot-Sionnest, P.; Wehrenberg, B.; Yu, D. Intraband Relaxation in CdSe Nanocrystals and the Strong Influence of the Surface Ligands. *J. Chem. Phys.* **2005**, *123*, 074709–074709.
48. Dolai, S.; Nimmala, P. R.; Mandal, M.; Muhoberac, B. B.; Dria, K.; Dass, A.; Sardar, R. Isolation of Bright Blue Light-Emitting CdSe Nanocrystals with 6.5 kDa Core in Gram Scale: High Photoluminescence Efficiency Controlled by Surface Ligand Chemistry. *Chem. Mater.* **2014**, *26*, 1278–1285.
49. Wang, Y.; Zhang, Y.; Wang, F.; Giblin, D. E.; Hoy, J.; Rohrs, H. W.; Loomis, R. A.; Buhro, W. E. The Magic-Size Nanocluster $(CdSe)_{34}$ as a Low-Temperature Nucleant for Cadmium Selenide Nanocrystals; Room-Temperature Growth of Crystalline Quantum Platelets. *Chem. Mater.* **2014**, *26*, 2233–2243.
50. Kasuya, A.; Sivamohan, R.; Barnakov, Y. A.; Dmitruk, I. M.; Nirasawa, T.; Romanyuk, V. R.; Kumar, V.; Mamykin, S. V.; Tohji, K.; Jeyadevan, B.; et al. Ultra-Stable Nanoparticles of CdSe Revealed from Mass Spectrometry. *Nat. Mater.* **2004**, *3*, 99–102.
51. Puzder, A.; Williamson, A. J.; Gygi, F.; Galli, G. Self-Healing of CdSe Nanocrystals: First-Principles Calculations. *Phys. Rev. Lett.* **2004**, *92*, 217401.
52. Kilina, S.; Ivanov, S.; Tretiak, S. Effect of Surface Ligands on Optical and Electronic Spectra of Semiconductor Nanoclusters. *J. Am. Chem. Soc.* **2009**, *131*, 7717–7726.
53. Fischer, S. A.; Crotty, A. M.; Kilina, S. V.; Ivanov, S. A.; Tretiak, S. Passivating Ligand and Solvent Contributions to the Electronic Properties of Semiconductor Nanocrystals. *Nanoscale* **2012**, *4*, 904–914.
54. Liu, I. S.; Lo, H.-H.; Chien, C.-T.; Lin, Y.-Y.; Chen, C.-W.; Chen, Y.-F.; Su, W.-F.; Liou, S.-C. Enhancing Photoluminescence Quenching and Photoelectric Properties of CdSe Quantum Dots with Hole Accepting Ligands. *J. Mater. Chem.* **2008**, *18*, 675–682.
55. Liu, J.; Neukirch, A. J.; Prezhdo, O. V. Phonon-Induced Pure-Dephasing of Luminescence, Multiple Exciton Generation, and Fission in Silicon Clusters. *J. Chem. Phys.* **2013**, *139*, 164303.
56. Mukamel, S. *Principles of Nonlinear Optical Spectroscopy*; Oxford University Press: New York, 1995.
57. Bawendi, M. G.; Wilson, W. L.; Rothberg, L.; Carroll, P. J.; Jedju, T. M.; Steigerwald, M. L.; Brus, L. E. Electronic Structure and Photoexcited-Carrier Dynamics in Nanometer-Size CdSe Clusters. *Phys. Rev. Lett.* **1990**, *65*, 1623–1626.
58. Nirmal, M.; Murray, C. B.; Bawendi, M. G. Fluorescence-Line Narrowing in CdSe Quantum Dots: Surface Localization of the Photogenerated Exciton. *Phys. Rev. B: Condens. Matter Mater. Phys.* **1994**, *50*, 2293–2300.
59. Empedocles, S. A.; Bawendi, M. G. Influence of Spectral Diffusion on the Line Shapes of Single CdSe Nanocrystallite Quantum Dots. *J. Phys. Chem. B* **1999**, *103*, 1826–1830.
60. Cordero, S. R.; Carson, P. J.; Estabrook, R. A.; Strouse, G. F.; Buratto, S. K. Photo-Activated Luminescence of CdSe Quantum Dot Monolayers. *J. Phys. Chem. B* **2000**, *104*, 12137–12142.
61. Salvador, M. R.; Hines, M. A.; Scholes, G. D. Exciton−Bath Coupling and Inhomogeneous Broadening in the Optical Spectroscopy of Semiconductor Quantum Dots. *J. Chem. Phys.* **2003**, *118*, 9380–9388.
62. Salvador, M. R.; Graham, M. W.; Scholes, G. D. Exciton-Phonon Coupling and Disorder in the Excited States of CdSe Colloidal Quantum Dots. *J. Chem. Phys.* **2006**, *125*, 184709.
63. Ellingson, R. J.; Beard, M. C.; Johnson, J. C.; Yu, P.; Micic, O. I.; Nozik, A. J.; Shabaev, A.; Efros, A. L. Highly Efficient Multiple Exciton Generation in Colloidal PbSe and PbS Quantum Dots. *Nano Lett.* **2005**, *5*, 865–871.
64. Habenicht, B. F.; Kalugin, O. N.; Prezhdo, O. V. *Ab initio* Study of Phonon-Induced Dephasing of Electronic Excitations in Narrow Graphene Nanoribbons. *Nano Lett.* **2008**, *8*, 2510–2516.
65. Kilina, S.; Kilin, D.; Tretiak, S. Light-Driven and Phonon-Assisted Dynamics in Organic and Semiconductor Nanostructures. *Chem. Rev.* **2015**, *115*, 5929–5978.
66. Kilina, S. V.; Kilin, D. S.; Prezhdo, V. V.; Prezhdo, O. V. Theoretical Study of Electron-Phonon Relaxation in PbSe and CdSe Quantum Dots: Evidence for Phonon Memory. *J. Phys. Chem. C* **2011**, *115*, 21641–21651.
67. Kamisaka, H.; Kilina, S. V.; Yamashita, K.; Prezhdo, O. V. *Ab initio* Study of Temperature- and Pressure Dependence of Energy and Phonon-Induced Dephasing of Electronic Excitations in CdSe and PbSe Quantum Dots. *J. Phys. Chem. C* **2008**, *112*, 7800–7808.
68. Mittleman, D. M.; Schoenlein, R. W.; Shiang, J. J.; Colvin, V. L.; Alivisatos, A. P.; Shank, C. V. Quantum Size Dependence of Femtosecond Electronic Dephasing and Vibrational Dynamics in CdSe Nanocrystals. *Phys. Rev. B: Condens. Matter Mater. Phys.* **1994**, *49*, 14435–14447.
69. Skinner, J. Theory of Pure Dephasing in Crystals. *Annu. Rev. Phys. Chem.* **1988**, *39*, 463–478.
70. Kresse, G.; Furthmüller, J. Efficiency of *ab-initio* Total Energy Calculations for Metals and Semiconductors Using a Plane-Wave Basis Set. *Comput. Mater. Sci.* **1996**, *6*, 15–50.
71. Long, R.; English, N. J.; Prezhdo, O. V. Photo-Induced Charge Separation Across the Graphene−TiO2 Interface is Faster than Energy Losses: A Time-Domain *ab initio* Analysis. *J. Am. Chem. Soc.* **2012**, *134*, 14238–14248.

72. Blöchl, P. E. Projector Augmented-Wave Method. *Phys. Rev. B: Condens. Matter Mater. Phys.* **1994**, *50*, 17953–17979.
73. Perdew, J. P.; Burke, K.; Ernzerhof, M. Generalized Gradient Approximation Made Simple. *Phys. Rev. Lett.* **1996**, *77*, 3865–3868.
74. Vanderbilt, D. Soft Self-Consistent Pseudopotentials in a Generalized Eigenvalue Formalism. *Phys. Rev. B: Condens. Matter Mater. Phys.* **1990**, *41*, 7892–7895.
75. Fischer, S. A.; Habenicht, B. F.; Madrid, A. B.; Duncan, W. R.; Prezhdo, O. V. Regarding the Validity of the Time-Dependent Kohn−Sham Approach for Electron-Nuclear Dynamics *via* Trajectory Surface Hopping. *J. Chem. Phys.* **2011**, *134*, 024102.